Check for updates

ADVANCED FUNCTIONAL MATERIALS
www.afm-journal.de

$Al_{1-x}Sc_xN$-Based Ferroelectric Domain-Wall Memristors

*Haidong Lu, Georg Schönweger, Niklas Wolff, Ziming Ding, Adrian Petraru, Isabel Streicher, Hermann Kohlstedt, Christian Kübel, Stefano Leone, Lorenz Kienle, Simon Fichtner, and Alexei Gruverman**

Emerging wurzite-structured ferroelectrics can help satisfy the demand for high-performance ferroelectrics compatible with III-nitride and Si technology. One of their particularly appealing properties is related to the presence of conducting domain walls, which can be used as functional elements in the devices with electrically tunable resistance–memristors. Using a combination of piezoresponse force microscopy (PFM) and conductive atomic force microscopy (CAFM) techniques, the electrical conductivity of the head-to-head (H-H) domain walls in the $Al_{0.85}Sc_{0.15}N$ thin films on the n-GaN substrate is directly demonstrated. Transmission electron microscopy (TEM) studies of the $Al_{0.85}Sc_{0.15}N$ films reveal that the conducting nature of these domain walls is likely related to their inclination with respect to the polar axis, resulting in polarization discontinuity at the domain junctions. On the other hand, no increased conductivity has been detected for the tail-to-tail (T-T) domain walls reflecting a semiconducting nature of $Al_{0.85}Sc_{0.15}N$ thin films. Modulation of the domain wall density by voltage pulses with varying amplitude or duration allows realization of multiple stable resistance states with the maximum ON/OFF ratio of over 1500. These findings pave the way for the next-generation of ferroelectric electronic devices compatible with III-nitride technology.

1. Introduction

Demonstration of ferroelectricity in the wurtzite-structured AlN-ScN solid solutions[1] enables integration of the ferroelectric materials into the III-nitride semiconductor and Si technology for future electronic device applications.[2] An especially intriguing phenomenon that has been reported in a number of ferroelectrics[3] but only recently observed in $Al_{1-x}Sc_xN$ films[4,5] is the electrical conductivity of the domain walls. Effective control of the domain wall density and modulation of their transport behavior by electrical means makes them attractive for use as functional elements in electrically tunable devices.[6] Recent transmission electron microscopy studies reveal stable inclined domain walls of the head-to-head (H-H) and tail-to-tail (T-T) type in the ultrathin $Al_{1-x}Sc_xN$ films.[5] Other studies have attributed the tunable resistance observed in the $Al_{1-x}Sc_xN$ capacitors

H. Lu, A. Gruverman
Department of Physics and Astronomy
University of Nebraska
Lincoln, NE 68588, USA
E-mail: agruverman2@unl.edu

G. Schönweger, S. Fichtner
Fraunhofer Institute of Silicon Technology (ISIT)
Fraunhoferstraße 1, 25524 Itzehoe, Germany

G. Schönweger, N. Wolff, L. Kienle, S. Fichtner
Department of Material Science
Kiel University
Kaiserstraße 2, D-24143 Kiel, Germany

N. Wolff
Kiel Nano
Surface and Interface Science (KiNSIS)
Kiel University
24118 Kiel, Germany

The ORCID identification number(s) for the author(s) of this article can be found under https://doi.org/10.1002/adfm.202503143

Z. Ding, C. Kübel
Advanced Electron Microscopy in Materials Research
Institute of Nanotechnology (INT)
Karlsruhe Institute of Technology (KIT)
76344 Eggenstein-Leopoldshafen, Germany

Z. Ding, C. Kübel
Karlsruhe Nano Micro Facility (KNMFi)
Karlsruhe Institute of Technology (KIT)
76344 Eggenstein-Leopoldshafen, Germany

A. Petraru, H. Kohlstedt
Department of Electrical and Information Engineering
Kiel University
Kaiserstr. 2, 24143 Kiel, Germany

I. Streicher
Consiglio Nazionale delle Ricerche–Istituto per la Microelettronica e Microsistemi (CNR-IMM)
Strada VIII n. 5 – Zona Industriale, Catania 95121, Italy

S. Leone
Fraunhofer Institute for Applied Solid State Physics IAF
Tullastrasse 72, 79108 Freiburg, Germany

© 2025 The Author(s). Advanced Functional Materials published by Wiley-VCH GmbH. This is an open access article under the terms of the Creative Commons Attribution-NonCommercial-NoDerivs License, which permits use and distribution in any medium, provided the original work is properly cited, the use is non-commercial and no modifications or adaptations are made.

DOI: 10.1002/adfm.202503143

16163028, 0, Downloaded from https://advanced.onlinelibrary.wiley.com/doi/10.1002/adfm.202503143 by Karlsruher Institut Für Technologie, Wiley Online Library on [11/08/2025]. See the Terms and Conditions (https://onlinelibrary.wiley.com/terms-and-conditions) on Wiley Online Library for rules of use; OA articles are governed by the applicable Creative Commons License

to the conducting behavior of such domain walls.[4,5] However, no direct observation of the domain wall conductivity in $Al_{1-x}Sc_xN$ has been reported so far. Addressing this issue is critical for understanding the mechanism of the domain wall transport properties and their device application.

Recent structural studies reveal that single-crystalline $Al_{1-x}Sc_xN$ thin films grown by metal organic chemical vapor deposition (MOCVD) show significantly higher structural quality than the sputter-deposited films could demonstrate so far.[7,8] This makes the MOCVD grown $Al_{1-x}Sc_xN$ films an ideal host for studying the tunable resistive behavior associated with varying domain structures. In this work, measurements have been carried out using 230-nm-thick single-crystalline $Al_{0.85}Sc_{0.15}N$ films grown by MOCVD. It has been found that multiple resistance states can be achieved in the $Al_{0.85}Sc_{0.15}N$ capacitors by inducing step-by-step polarization switching via successive application of voltage pulses. Each individual resistance state can be programmed by varying the pulse amplitude or duration, resulting in a pre-history dependent memristive behavior with a maximum ON/OFF ratio of over 1500. Piezoresponse force microscopy (PFM) imaging, scanning transmission electron microscopy (STEM) investigation, and electrical characterization of the generated domain structures reveal the direct correlation between the density of the domain walls and device resistance. Characterization by conductive atomic force microscopy (CAFM) provides direct evidence for the high conductivity of these domain walls, demonstrating their main role as the functional elements in the memristive device's functionality. STEM imaging of the partially switched cross-cut capacitors reveals a number of slanted domain walls separating the head-to-head (H-H) domain junctions, i.e., interfaces between two neighboring regions where the polarization vectors face toward each other. This implies that the polarization discontinuity and the associated charge accumulation at the H-H domain walls are the physical mechanism behind their conductance. These findings provide a tangible reason for comprehensive fundamental and applied studies of the domain walls in the $Al_{1-x}Sc_xN$ structures to further extend the prospects of using the wurtzite ferroelectrics in III-nitride and Si technology.

2. Results and Discussion

2.1. Sample Preparation and Characterization

Details of the 230-nm-thick $Al_{0.85}Sc_{0.15}N$ films growth by MOCVD on Si-doped GaN-on-sapphire templates are given in Materials and Methods. A specific Sc concentration of 15% has been chosen to alleviate the interfacial strain due to the lattice mismatch between the $Al_{1-x}Sc_xN$ and GaN layers.[9] To avoid post-growth oxidation, the $Al_{0.85}Sc_{0.15}N$ layer was capped in situ with a 10-nm-thick SiN layer followed by sputter-deposition of the 30-nm-thick Pt layer. Ion beam etching (IBE) has been used to pattern the top Pt electrodes, creating the $Pt/SiN/Al_{0.85}Sc_{0.15}N/n$-GaN capacitors of 10–30 µm in diameter. Capacitors investigated by STEM and CAFM have been switched 400 times, which was followed by application of a unipolar triangular voltage pulse of 133 V in amplitude to induce N-polarity (downward polarization). Further details about the polling process can be found elsewhere.[7] For the CAFM measurements, after pre-poling, the $Al_{0.85}Sc_{0.15}N$ layer was exposed by dry-etching the Pt and SiN layer.

2.2. Resistive Switching in the $Al_{0.85}Sc_{0.15}N$ Capacitors

Figure 1a–c displays the PFM images of the $Al_{0.85}Sc_{0.15}N$ capacitors corresponding to three different polarization states: a single-domain pristine M-polar state (upward polarization) (Figure 1a), a polydomain state resulting from application of a 110 V, 0.1 s pulse (Figure 1b), and a single-domain N-polar state (downward polarization) arising after application of a 125 V, 0.1 s pulse (Figure 1c). The corresponding steady-state *I–V* curves in Figure 1d show that the polydomain state exhibits the highest conductivity in agreement with the previous studies of the resistive switching behavior in the sputtered $Al_{1-x}Sc_xN$ films.[4] This behavior, along with the imbalance between the resistances of the capacitor in the upward and downward polarization states, is a clear indication that the presence or absence of the domain walls, which must be conductive, is a major factor in the resistive switching behavior of the $Al_{0.85}Sc_{0.15}N$ capacitors. It should be noted that the polarization-coupled change in the interface Schottky barrier height[10] could also contribute to the resistive switching effect. However, it cannot cause the non-monotonic resistance change shown in Figure 1a–d. On top of this, the *I–V* curves are far more symmetric than could be expected from the barrier-originating resistive switching.

A more detailed look into the resistive switching reveals a possibility of fine tuning of device resistance by modulating the write pulse amplitude or the number of write pulses. Figure 1e,f show the steady-state *I–V* curves and the device current density as a function of the write pulse amplitude that switches the polarization from the full M- to the (partial) N-polar state (prior to the application of each write pulse, the capacitor was reset into the full M-polar state). The device conductivity starts to increase at 86 V, which corresponds to the onset of polarization reversal, and reaches its maximum level in the middle of the switching process at 92 V with the capacitor set into a polydomain state. Further increase in the write pulse amplitude results in a gradual decrease of the current density, reaching a constant value when polarization switching is complete, and the sample returns to a monodomain state. The maximum ON/OFF resistance ratio achieved in this process exceeds 1500, which is more than sufficient for potential device applications. A similar conductance tunability can be realized by performing cumulative switching, i.e., by consecutive application of a number of write pulses with the same amplitude (Figure 1g). The obtained resistive switching behavior provides a basis for employing the $Al_{1-x}Sc_xN$ memristors in neuromorphic circuits.[11]

2.3. STEM Imaging of the $Al_{0.85}Sc_{0.15}N$ Capacitors

The structural quality of the MOCVD grown $Al_{1-x}Sc_xN$ films allows for in-depth studies of the field-induced domain structures by STEM.[12] **Figure 2a,b** presents a large field-of-view ABF-STEM image showing a zig-zag H-H boundary separating the switched N-polar and pristine M-polar regions at the capacitor edge. Investigation by atomic resolution iDPC-STEM is used to identify

© 2025 The Author(s). Advanced Functional Materials published by Wiley-VCH GmbH

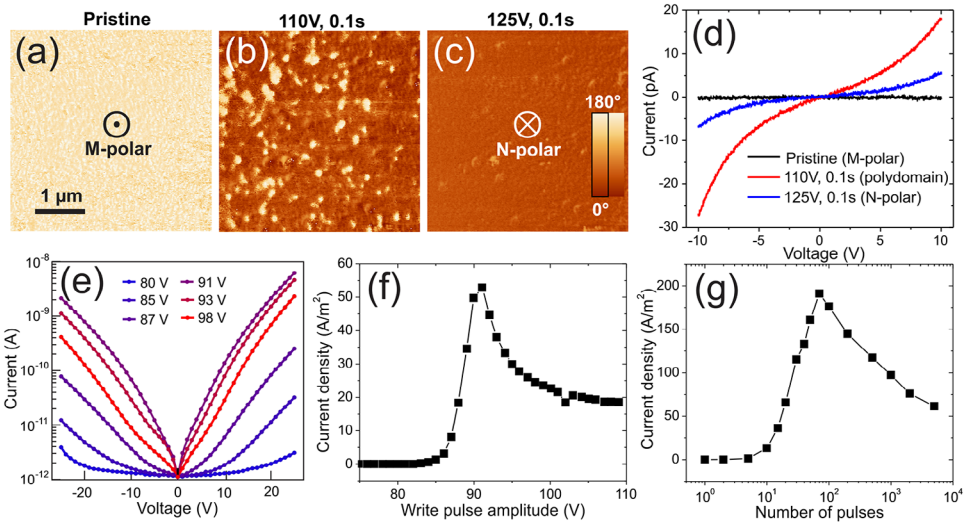

Figure 1. Resistive switching in the $Al_{0.85}Sc_{0.15}N$ capacitors. a–c) PFM phase images of the (a) pristine M-polar (upward polarization) state, (b) after application of the 110 V, 0.1s pulse, showing a polydomain state, and (c) after application of 125 V, 0.1 s pulse, showing a N-polar (downward polarization) state. d) *I–V* curves of the pristine M-polar, polydomain, and N-polar states corresponding to the states in (a–c). e,f) Steady-state *I–V* curves (e) and steady-state current density extracted at −40 V (f) in the $Al_{0.85}Sc_{0.15}N$ capacitor as a function of the write pulse amplitude. The pulse width was 0.1 s. After application of each write pulse the device was reset into the full M-polar state by application of −110 V bias for 0.5 s. g) Steady-state current density at −40 V measured in the $Al_{0.85}Sc_{0.15}N$ capacitor as a function of the number of 110 V, 1 ms write pulses (cumulative switching). The measurements were performed on a pristine ((a–d) and (g)) as well as on a pre-cycled capacitors ((e-f) – see sample preparation). This results in a slight variation of the write voltage required for tuning the conductivity due to the imprint variations upon cycling.[17]

the local polarity on the unit cell level as well as the domain wall position and its inclination angle. These studies confirm the M-polarity of the pristine $Al_{0.85}Sc_{0.15}N$ film next to the capacitor edge (Figure 2b) and a pinned layer close to the bottom interface in the switched region. Figure 2c shows a magnified view of a ≈1 nm wide H-H domain wall between the M-polar domain (left side) and the N-polar domain (right side) with an inclination angle of ≈15°. Moreover, residual nanosized areas with M-polarity (Figure 2d) are revealed within the switched N-polar region (Figure 2e) where the film surface is covered by Pt residues from the electrode patterning. This observation suggests incomplete and inhomogeneous switching at the capacitor edges, resulting in a locally increased density of surface-near domain walls.

Stability of the H-H domain walls is determined by proper screening of polarization via charge accumulation, which implies that the $Al_{0.85}Sc_{0.15}N$ films used in this study are slightly n-doped and negative charges are the majority carriers. Note that there is no need for the domain walls to extend from the top to the bottom interfaces to exhibit a high conductivity, as the carriers driven by the applied bias will diffuse out of the domain wall, reaching the bottom electrode. Given a high electron mobility in AlScN of the order of $\approx 10^2$ cm^2 (V s)$^{-1}$, a diffusion coefficient of 0.01 cm^2 s^{-1} can be estimated from the Einstein relation that would yield a diffusion length of the order of 10 μm within 1 μs. Therefore, it is reasonable to assume that a current signal could be detected from the charged domain wall even if it does not extend across the entire film thickness. A similar conducting behavior was observed in the 500-nm-thick $LiNbO_3$ crystals, where the inclined charged domain walls induced at the top surface did not reach the bottom electrode.[13]

2.4. CAFM Imaging of the Free Surface of $Al_{0.85}Sc_{0.15}N$

Direct studies of the local domain wall conductivity have been carried out by CAFM imaging of the exposed surface of the $Al_{0.85}Sc_{0.15}N$ film. To prepare for these measurements, the capacitors have been pre-poled into the N-polar state (downward polarization) with subsequent removal of the top electrode by IBE (see Materials and Methods), as shown in the schematic drawing in **Figure** 3e. The topographic image in Figure 3a shows a capacitor edge after etching, where the area outside of the etched electrode is also slightly etched, creating a height difference of ≈25 nm. PFM imaging of the same region (Figure 3b) shows the N-polar state in the capacitor area and the M-polar pristine state outside it, which, according to the STEM data in Figure 2, are separated by the H-H domain boundary. CAFM imaging of the same region (Figure 3c,d) reveals a significantly higher current signal along the H-H domain wall compared to the regions of uniform domains, confirming their dominant contribution as the conducting elements to the resistive switching behavior of the $Al_{0.85}Sc_{0.15}N$ capacitor in Figure 1. The insets in Figure 3c,d display the cross-sectional profiles along the dashed lines, showing that the N-polar domain shows a current roughly twice as small as on the H-H domain wall, while no detectable current is recorded from the M-polar domain. Note that the CAFM imaging does not affect the domain structure, suggesting that no polarization switching is associated with the measured current signals. Local *I–V* spectroscopy of the domain wall as well as of the M- and N-polar domains shown in Figure 3f is consistent with the CAFM imaging results, revealing at the same time their asymmetric transport behavior. This asymmetry and difference in conductivity for the M- and N-polar states may be

© 2025 The Author(s). Advanced Functional Materials published by Wiley-VCH GmbH

16163028, 0, Downloaded from https://advanced.onlinelibrary.wiley.com/doi/10.1002/adfm.202503143 by Karlsruher Institut Für Technologie, Wiley Online Library on [11/08/2025]. See the Terms and Conditions (https://onlinelibrary.wiley.com/terms-and-conditions) on Wiley Online Library for rules of use; OA articles are governed by the applicable Creative Commons License

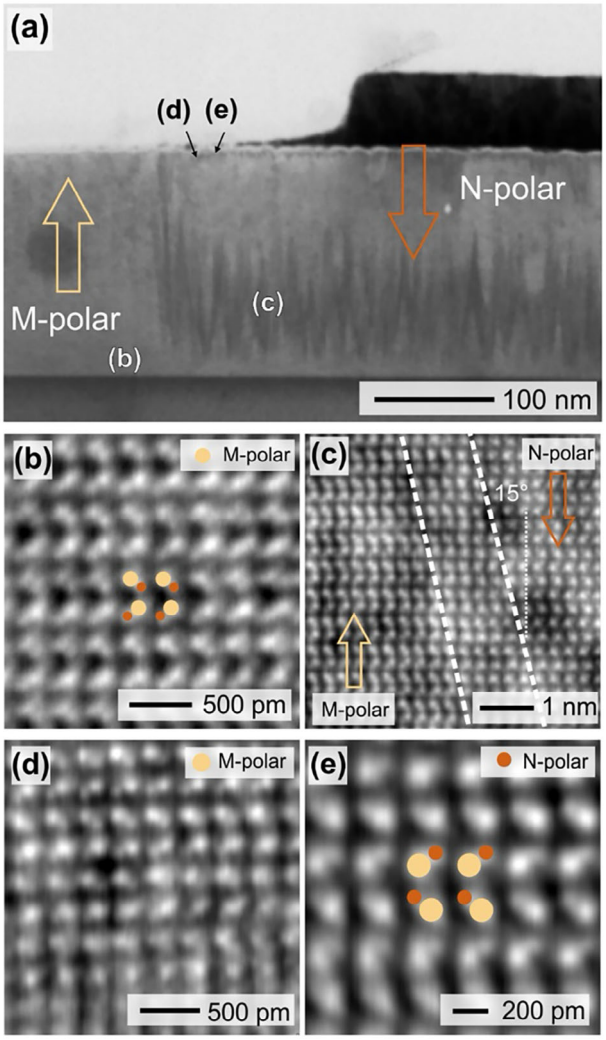

Figure 2. STEM investigations of polar domain structures at the edge of an N-poled capacitor showing wedge-shaped downward domains next to the upward polarized pristine region outside and near the $Al_{0.85}Sc_{0.15}N$/GaN interface. a) ABF-STEM image of the capacitor edge. b,c) iDPC images display the atomic polarity present (b) outside of the switched region, (c) at the inclined H-H domain boundary, and (d,e) near the upper interface.

associated with the polarization-dependent Schottky barrier height at the tip-sample interface[10] or residual conductive domain walls which are pinned at the lower interface of the film.[7] It is worth mentioning that the CAFM data in Figure 3 were acquired several weeks after poling, which indicates remarkable stability of the charged domain walls and strong retention of the induced resistive states.

To investigate the difference in the conducting behavior of the H-H and T-T domain walls, a negative bias was applied to the N-polar (downward) surface of the $Al_{0.85}Sc_{0.15}N$ film through the PFM tip. This procedure should result in the formation of the M-polar (upward) domain, presumably bounded by the T-T domain wall, since domain nucleation should be induced at the top interface due to the field distribution originating from the tip (a schematic drawing of the resulting M-polar domain is shown in).

Figure 4a–d shows a comparison of PFM and CAFM images before (Figure 4a,b) and after (Figure 4c,d) application of several −65 V, 1 s pulses to different locations on the film surface. It can be seen that the high conductive state of the H-H domain wall is erased locally due to the local polarization reversal by negative bias application. Similarly, the formation of the M-polar domain within the N-polar area is accompanied by a local conductance decrease. Although it is difficult to deconvolute the effect of the Schottky barrier change at the interface from the domain wall conductance effect, it could still be concluded with a high degree of certainty that the T-T domain walls are much less conductive. A similar difference in the conducting behavior of the H-H and T-T domain walls reported previously in $BaTiO_3$ and $LiNbO_3$ crystals[14] has been attributed to the accumulation of the free electronic charges or mobile defects at the strongly inclined H-H boundaries, which carry a positive bound charge resulting from polarization discontinuity. Assuming n-type conductivity, the same mechanism for domain wall conductance could be invoked in the studied $Al_{0.85}Sc_{0.15}N$ samples, although a significant modification of the electronic structure at the domain walls could also be considered. In addition, different concentrations and mobilities of negative and positive compensating charges could also lead to different conductivities of the H-H and T-T domain walls.

3. Conclusion

The electrical conductivity of the H-H domain walls has been directly demonstrated by CAFM imaging and local *I–V* spectroscopy measurements. STEM imaging reveals that the H-H oriented domain walls created at the capacitor edge have an inclination angle of ≈15°, resulting in polarization divergence at the wall junctions and their conducting behavior. In contrast, the T-T domain walls created by the local pulse application do not show any significant conductivity. The obtained results could lead to an expansion of the application range of the $Al_{1-x}Sc_xN$-based devices by employing conductive domain walls as functional elements, allowing programmable control of multilevel resistance states and enabling memristive functionalities.

4. Experimental Section

Sample Preparation: A MOCVD reactor equipped with a proprietary, heated gas supply system for low-vapor-pressure Sc precursors was used for the film growth. The Sc precursor chosen for this work was $(EtCp)_2Sc(bdma)$, which can be operated by keeping the source material at 100 °C. The $Al_{0.85}Sc_{0.15}N$ layer was capped in situ with a SiN_x layer in order to avoid post-growth oxidation, as described elsewhere.[15] The layers were characterized by means of optical microscopy, atomic force microscopy, high-resolution X-ray diffraction, and secondary ions mass spectrometry.[7] A 30-nm-thick Pt top layer was deposited by sputter-deposition using an Oerlikon (now Evatec) MSQ 200 multisource system.[16] The top electrodes were structured by ion beam etching (IBE, Oxford Instruments Ionfab 300). Of importance for this study is the fact that shadowing during IBE leads to a thin Pt residue area of ≈100–200 nm in width around the capacitor edge (Figure 2a), which resulted in a poly-domain state at the capacitor edge

TEM Imaging: High-resolution scanning transmission electron microscopy (HRSTEM) imaging was conducted on the double-corrected transmission electron microscope (Themis Z, Thermo Fisher) at an

© 2025 The Author(s). Advanced Functional Materials published by Wiley-VCH GmbH

16163028, 0, Downloaded from https://advanced.onlinelibrary.wiley.com/doi/10.1002/adfm.202503143 by Karlsruher Institut Für Technologie, Wiley Online Library on [11/08/2025]. See the Terms and Conditions (https://onlinelibrary.wiley.com/terms-and-conditions) on Wiley Online Library for rules of use; OA articles are governed by the applicable Creative Commons License

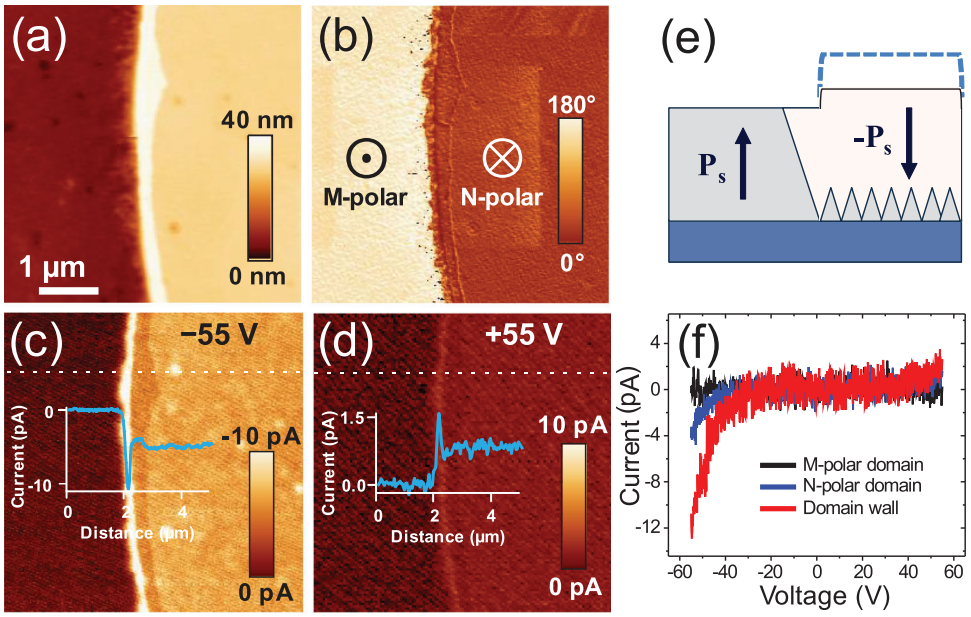

Figure 3. PFM and CAFM imaging of the free film surface near the pre-poled $Al_{0.85}Sc_{0.15}N$ capacitor edge after etching away the top electrode. a) Topographic image of the capacitor edge after etching. b) PFM phase image of N-polar (downward polarization) domain in the capacitor area where the top electrode was present, and the M-polar (upward polarization) domain outside of it. The capacitor was pre-poled with +133 V before etching. c,d) CAFM images of the same area as in (a) and (b) using a −55 V (c) and +55 V (d) dc bias applied to the bottom electrode. The insets show the cross-sectional profiles along the dashed lines. e) Schematic drawing of the cross-sectional domain profile after the top electrode was etched. The top electrode position before etching is marked by a dashed line. f) *I–V* curves measured on the M- and N-polar domains, and on the H-H domain wall.

acceleration voltage of 300 kV, which enables the resolution of ≈75 pm. The convergence angle of the electron beam was 30 mrad, while the screen current was ≈80–200 pA. Integrated differential phase contrast (iDPC) HRSTEM images were collected by segmented detectors at the collection angles between 6 and 23 mrad, enabling to imaging the nitrogen atom positions. In addition, the annular bright field (ABF) imaging and DPC mapping for the microscale domain nature were done using the electron beam with a convergence angle of 10 mrad, and the collection angle range is 3–17 mrad.

Electrical Characterization: Ferroelectric characterization and poling were performed using an aixACCT TF Analyzer 2000. Capacitors investigated by CAFM and STEM were switched 400 times by applying a voltage signal with triangular waveform at a frequency of 1.5 kHz and 143 V amplitude with an offset of −10 V. Subsequently, the capacitor was switched to N-polarity by applying a unipolar triangular pulse of 133 V. Steady-state current measurements were performed using a Keithley 6487 Picoammeter/Voltage source. Rectangular write and erase pulses were applied to the capacitors. The readout was performed by sweeping a staircase voltage signal with a step size of 1 V and a hold time of 0.6 s after which the steady state current was measured. The voltage signal was applied to the top electrode. The *I–V* spectroscopy measurements have been carried out at 1 Hz with the sweeping bias applied to the bottom electrode.

PFM and CAFM Imaging: PFM and CAFM measurements were carried out using a commercial AFM system (MFP-3D, Asylum Research, Oxford Instruments) using Pt-coated conductive probes (NSC18/Pt, Mikromasch). A dual AC resonance-enhanced mode was employed for the PFM imaging using an AC modulation voltage with an amplitude of 1 V at 390 kHz applied to the tip. The CAFM imaging and *I–V* spectroscopy measurements were performed using the ORCA module with a DC bias applied to the bottom electrode.

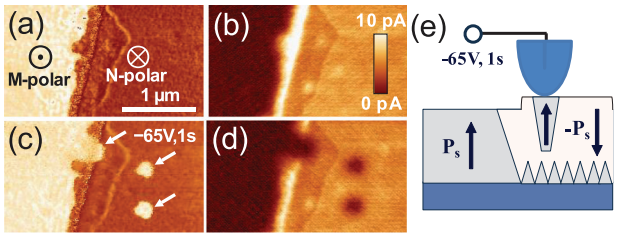

Figure 4. PFM and CAFM imaging of the free film surface near the pre-poled $Al_{0.85}Sc_{0.15}N$ capacitor edge before and after local tip-induced switching. a–d) PFM (a,c) and CAFM images (b,d) of the initial state (a,b) and after application of several −65 V, 1 s voltage pulses (c,d). Locations where the pulses were applied, are shown by the arrows in (c). e) Schematic illustration of the tip-induced writing of the upward domain bounded by the T-T walls.

Acknowledgements

This work was supported by the UNL Grand Challenges catalyst award "Quantum Approaches Addressing Global Threats." This work was also supported by the Deutsche Forschungsgemeinschaft (DFG) under the scheme of the Collaborative Research Center (CRC) 1261 – Project ID 286471992, Project ID 458372836, and Project ID 434434223 – SFB 1461. The authors acknowledge financial support by the Federal Ministry of Education and Research (BMBF) under project 03VP10842 (VIP+ FeelScreen) and the European Union (FIXIT, GA 101135398). Views and opinions expressed are, however, those of the author(s) only and do not necessarily reflect those of the European Union or the European Research Council Executive Agency. In addition, the authors are grateful to the Karlsruhe Nano Micro Facility (KNMFi) at KIT for providing TEM access.

Conflict of Interest

The authors declare no conflicts of interest.

© 2025 The Author(s). Advanced Functional Materials published by Wiley-VCH GmbH

16163028, 0, Downloaded from https://advanced.onlinelibrary.wiley.com/doi/10.1002/adfm.202503143 by Karlsruher Institut Für Technologie, Wiley Online Library on [11/08/2025]. See the Terms and Conditions (https://onlinelibrary.wiley.com/terms-and-conditions) on Wiley Online Library for rules of use; OA articles are governed by the applicable Creative Commons License

Data Availability Statement

The data that support the findings of this study are available from the corresponding author upon reasonable request.

Keywords

domain wall conductivity, ferroelectric AlScN, ferroelectric memristor, resistive switching

Received: March 8, 2025
Revised: May 14, 2025
Published online:

[1] S. Fichtner, N. Wolff, F. Lofink, L. Kienle, B. Wagner, *J. Appl. Phys.* **2019**, *125*, 114103.
[2] a) T. Mikolajick, S. Slesazeck, H. Mulaosmanovic, M. H. Park, S. Fichtner, P. D. Lomenzo, M. Hoffmann, U. Schroeder, *J. Appl. Phys.* **2021**, *129*, 100901; b) Y. Zhang, Q. Zhu, B. Tian, C. G. Duan, *Nano-Micro Lett.* **2024**, *16*, 227.
[3] a) J. Seidel, L. W. Martin, Q. He, Q. Zhan, Y.-H. Chu, A. Rother, M. E. Hawkridge, P. Maksymovych, P. Yu, M. Gajek, N. Balke, S. V. Kalinin, S. Gemming, F. Wang, G. Catalan, J. F. Scott, N. A. Spaldin, J. Orenstein, R. Ramesh, *Nat. Meter.* **2009**, *8*, 229; b) J. Guyonnet, I. Gaponenko, S. Gariglio, P. Paruch, *Adv. Mater.* **2011**, *23*, 5377; c) M. Schröder, A. Haußmann, A. Thiessen, E. Soergel, T. Woike, L. M. Eng, *Adv. Funct. Mater.* **2012**, *22*, 3936; d) D. Meier, J. Seidel, A. Cano, K. Delaney, Y. Kumagai, M. Mostovoy, N. A. Spaldin, R. Ramesh, M. Fiebig, *Nat. Mater.* **2012**, *11*, 284.
[4] H. Lu, G. Schönweger, A. Petraru, H. Kohlstedt, S. Fichtner, A. Gruverman, *Adv. Funct. Mater.* **2024**, *34*, 2315169.
[5] G. Schönweger, N. Wolff, M. R. Islam, M. Gremmel, A. Petraru, L. Kienle, H. Kohlstedt, S. Fichtner, *Adv. Sci.* **2023**, *10*, 2302296.
[6] a) G. Catalan, J. Seidel, R. Ramesh, J. F. Scott, *Rev. Mod. Phys.* **2012**, *84*, 119; b) D. Meier, *J. Phys. Cond. Matter.* **2015**, *27*, 463003.
[7] N. Wolff, G. Schönweger, I. Streicher, M. R. Islam, N. Braun, P. Stranák, L. Kirste, M. Prescher, A. Lotnyk, H. Kohlstedt, S. Leone, L. Kienle, S. Fichtner, *Adv. Phys. Res.* **2024**, *3*, 2300113.
[8] a) I. Streicher, S. Leone, C. Manz, L. Kirste, M. Prescher, P. Waltereit, M. Mikulla, R. Quay, O. Ambacher, *Cryst. Growth Des.* **2023**, *23*, 782; b) I. Streicher, S. Leone, L. Kirste, C. Manz, P. Straňák, M. Prescher, P. Waltereit, M. Mikulla, R. Quay, O. Ambacher, *Phys. Status Solidi RRL* **2023**, *17*, 2200387; c) I. Streicher, S. Leone, M. Zhang, T. S. Tlemcani, M. Bah, P. Straňák, L. Kirste, M. Prescher, A. Yassine, D. Alquier, O. Ambacher, *Adv. Funct. Mater.* **2024**, *34*, 2403027.
[9] a) D. V. Dinh, J. Lähnemann, L. Geelhaar, O. Brandt, *Appl. Phys. Lett.* **2023**, *122*, 152103; b) S. Zhang, W. Y. Fu, D. Holec, C. J. Humphreys, M. A. Moram, *J. Appl. Phys.* **2013**, *114*, 243516.
[10] D. Wang, P. Wang, S. Mondal, S. Mohanty, T. Ma, E. Ahmadi, Z. Mi, *Adv. Electron. Mater.* **2022**, *8*, 2200005.
[11] S. Oh, H. Hwang, I. K. Yoo, *APL Mater.* **2019**, *7*, 091109.
[12] N. Wolff, T. Grieb, G. Schönweger, F. F. Krause, I. Streicher, S. Leone, A. Rosenauer, S. i. Fichtner, L. Kienle, *J. Appl. Phys.* **2025**, *137*, 084101.
[13] H. Lu, Y. Tan, J. P. V. McConville, Z. Ahmadi, B. Wang, M. Conroy, K. Moore, U. Bangert, J. E. Shield, L. Q. Chen, J. M. Gregg, A. Gruverman, *Adv. Mat.* **2019**, *31*, 1902890.
[14] T. Sluka, A. K. Tagantsev, P. Bednyakov, N. Setter, *Nat. Comm.* **2013**, *4*, 1808.
[15] J. Ligl, S. Leone, C. Manz, L. Kirste, P. Doering, T. Fuchs, M. Prescher, O. Ambacher, *J. Appl. Phys.* **2020**, *127*, 195704.
[16] G. Schönweger, M. R. Islam, N. Wolff, A. Petraru, L. Kienle, H. Kohlstedt, S. Fichtner, *Phys. Status Solidi RRL* **2023**, *17*, 2200312.
[17] M. Gremmel, S. Fichtner, *J. Appl. Phys.* **2024**, *135*, 204101.

© 2025 The Author(s). Advanced Functional Materials published by Wiley-VCH GmbH

16163028, 0, Downloaded from https://advanced.onlinelibrary.wiley.com/doi/10.1002/adfm.202503143 by Karlsruher Institut Für Technologie, Wiley Online Library on [11/08/2025]. See the Terms and Conditions (https://onlinelibrary.wiley.com/terms-and-conditions) on Wiley Online Library for rules of use; OA articles are governed by the applicable Creative Commons License